Identification of elastic properties from full-field measurements: a numerical study of the effect of filtering on the identification results

Mouldi Ben Azzouna, Pierre Feissel, Pierre Villon

Identification of elastic properties from full-field measurements: a numerical study of the effect of filtering on the identification results

Mouldi Ben Azzouna[1], **Pierre Feissel and Pierre Villon**

Laboratoire Roberval CNRS-UMR 7337, UTC, Centre de Recherche de Royallieu, BP 20529,
F-60205 Compiègne Cedex, France

E-mail: mouldi.ben-azzouna@utc.fr, pierre.feissel@utc.fr and pierre.villon@utc.fr

Abstract
The use of full-field displacement measurements in mechanical testing has increased dramatically over the last two decades. This is a result of the very rich information they provide, which is enabling new possibilities for the characterization of material constitutive parameters for inhomogeneous tests often based upon inverse approaches. Nonetheless, the measurement errors limit the accuracy of the identification of the constitutive parameters and their possible spatial resolution. The question addressed by this work is the following: can a filtering of the displacement measurement improve the results of the identification of elastic properties? The discussion is based on the study of a numerical example where the elastic parameters of an elastic structure with inhomogeneous properties are sought from synthetic data representative of in-plane full-field data. The displacement data are first filtered through a diffuse approximation algorithm, based on a moving least-squares approximation. Then, the identification of the elastic parameters is performed by an inverse approach based on the minimization of a cost function, defined as the least-squares gap between the experimental data and their numerical counterpart (finite element model updating). Within this framework, a first-order analysis is proposed in order to characterize the errors in the identified parameters, the measurement error characteristics being known. Results from raw and filtered displacement data are compared and discussed, filtering improving the identification for lower spatial resolution. The choice of the norm to define the gap between the experiment and the calculation is also discussed. For practical use and to take advantage of the proposed first-order methodology, two different ways can be considered: applying the methodology to a numerical example, representative of the experimental setup, to determine whether or not a filtering is valuable, and estimating the uncertainties of the identified parameters at the end of the identification process of an experimental characterization.

Keywords: diffuse approximation, full-field measurements, measurement perturbations, inverse identification

[1] Author to whom any correspondence should be addressed.

1. Introduction

The recent development of digitized full-field measurements opens new ways of characterizing materials in solid mechanics (Hild and Roux 2006, Kobayashi 1987), thanks to their richness, especially in the case of heterogeneous tests. Indeed, such tests are more and more performed by testing structures, heterogeneous materials or specimens under complex loading, where full-field measurements come fully into play. In particular, the identification of the elastic properties is frequently performed at various scales of observation, for example for composite materials (Gras *et al* 2012, Leclerc *et al* 2009), metallic materials (Zavattieri *et al* 2009), MEMS (Amiot *et al* 2006) and so on.

In this context, numerous identification methods were adapted or fully dedicated to the exploitation of full-field measurements in the framework of linear elasticity (Avril *et al* 2008b) in order to characterize the elastic properties of heterogeneous materials such as composites. Some procedures require strain fields whereas others deal with displacements.

However, the measurement errors cannot be ignored and may impair the identification results, especially in elasticity where signal-to-noise ratios are low. It could be all the more problematic when differentiating displacement data if strain fields are required, except for the case of techniques which provide the displacement derivatives directly, such as the grid method (Badulescu 2010) and the shearography technique (Francis *et al* 2007). Indeed, small measurement errors may induce large errors in the computed derivative (Geers *et al* 1996), because of the noise differentiation.

Many identification approaches manage uncertainty well, using different ways. We can cite the reconditioned equilibrium gap method (EGM) (Ben Azzouna *et al* 2011, Claire *et al* 2002, Roux and Hild 2008), which avoids noise differentiation, the virtual field method (VFM) (Grédiac *et al* 2006), based on the virtual work principle and allowing us to construct optimal virtual fields with respect to measurement perturbations, the integrated digital image correlation (I-DIC) (Réthoré *et al* 2009) which filters perturbations by performing image correlation with the addition of mechanical constraints and also the modified constitutive relation error (MCRE) method (Ben Azzouna *et al* 2013, Deraemaeker *et al* 2002, Feissel and Allix 2007, Ladevèze *et al* 1994) which takes into account both measurement perturbations and constitutive equation errors in the identification process. A review of recently developed methods for constitutive parameter identification based on kinematic full-field measurements is available in Avril *et al* (2008b).

Among identification methods, finite element model updating (FEMU) is the most intuitive and is used in a very large set of fields. Since it is based on the minimization of the least-squares gap between the experimental data and a standard finite element (FE) calculation, its implementation is straightforward and does not require special developments (Collins *et al* 1974, Cottin *et al* 1984, Hemez and Farhat 1993, Kavanagh and Clough 1971, Pagnacco *et al* 2005). Nevertheless, a standard FEMU approach proposes no particular treatment of measurement perturbations. In this paper, we discuss if the identification results by a FEMU approach can be improved by filtering the displacement measurements. A second question concerns the type of input data for the identification and the choice of the norm of the cost function.

To address the central question, we propose to perform a study on a numerical example, where some synthetic data are created from a 2D FE calculation taking into account a representative measurement random error. Within this framework, we can compare the identification results from raw and filtered data for the characterization of heterogeneous elastic properties. The filtering of the measurements is performed upstream of the identification stage. The choice here is to use a filtering approach based on local weighted least-squares minimization using a polynomial diffuse approximation (DA) (Avril *et al* 2008a, Nayroles *et al* 1991a). The identification is then performed with a FEMU method, leading to the minimization of a cost function with respect to the sought Lamé coefficients. Then, we should be able to define the relationship linking the identification error to the measurement error. We propose to characterize that relation through a first-order analysis. For practical use, the proposed first-order methodology can be applied as a pre-assessment study on a numerical example representative of the experimental setup, in order to determine whether or not a filtering is valuable. Furthermore, it can be applied to real test data, at the end of the identification process, in order to characterize the uncertainties of the identified parameters. For the sake of simplicity, thiswork only deals with synthetic data created by FE simulation.

The identification framework is first presented, defining the direct problem and the identification formulation, and the main theoretical properties of the filtering approach are recalled from Feissel (2012). Then, a first-order analysis connecting the identification error to the measurement perturbations is detailed and used to investigate the improvement of the identification of heterogeneous Lamé coefficients from the filtering through a numerical example. Eventually, the choice of the least-squares norm of the minimization step is discussed.

2. Identification framework and filtering method

This section describes the studied inverse problem and the filtering method used to reduce the perturbation effects on the identification results. The framework concerns the identification of distributed elastic properties by using kinematic measurements.

2.1. Identification framework

2.1.1. Direct problem and measurements. Let us consider a specimen with elastic isotropic properties, considered as heterogeneous. As sketched in figure 1, the specimen defined in a domain Ω is subjected to a mechanical loading and governed by the equations of continuum mechanics within the framework of plane stress assumption.

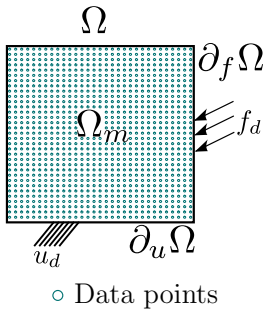

Figure 1. Reference problem related to the identification problem.

In the absence of body forces, the governing equations are

$$\begin{cases} \text{Equilibrium: } \underline{\text{div}}\,\underline{\underline{\sigma}} = \underline{0} \quad \text{in } \Omega & (1a) \\ \text{Kinematic compatibility: } \underline{\underline{\epsilon}} = \frac{1}{2}(\nabla\underline{u} + \nabla^{\mathsf{T}}\underline{u}) \quad \text{in } \Omega & (1b) \\ \text{Constitutive equation: } \underline{\underline{\sigma}} = \mathbb{C}\underline{\underline{\epsilon}} \quad \text{in } \Omega, & (1c) \end{cases}$$

with $\underline{u}$ the displacement vector, and $\underline{\underline{\sigma}}$ and $\underline{\underline{\epsilon}}$ respectively the Cauchy stress tensor and the infinitesimal strain tensor that depends on the displacement $\underline{u}$ (1b). $\mathbb{C}$ is an isotropic stiffness tensor, defined as a piecewise constant over the domain Ω and is described through the Lamé coefficients (λ, μ). For each homogeneous subset denoted by Ω_k, $k \in [1, N_c]$, with N_c the number of homogeneous subsets, under the plane stress assumption, the elasticity tensor is written as

$$\begin{aligned} \mathbb{C} &= \begin{bmatrix} \lambda_k^* + 2\,\mu_k & \lambda_k^* & 0 \\ \lambda_k^* & \lambda_k^* + 2\,\mu_k & 0 \\ 0 & 0 & 2\,\mu_k \end{bmatrix} \\ &= \frac{E_k}{1-\nu_k^2} \begin{bmatrix} 1 & \nu_k & 0 \\ \nu_k & 1 & 0 \\ 0 & 0 & 1-\nu_k \end{bmatrix}, \end{aligned} \tag{2}$$

where $\lambda^* = 2\,\lambda\,\mu/\lambda + 2\,\mu$. Young's modulus and Poisson's ratio are derived from the Lamé coefficients as

$$\nu = \frac{\lambda}{2(\lambda+\mu)}; \quad E = \mu\,\frac{(3\lambda+2\mu)}{\lambda+\mu}. \tag{3}$$

The Lamé coefficients of all the subsets are collected in a vector $\underline{\theta}$, of length denoted by p. $\underline{\theta}$ will be the unknown of the identification problem.

The above mechanical problem has mixed boundary conditions, partitioned over two border types:

$$\begin{cases} \text{Neumann boundary conditions: } \underline{\underline{\sigma}}.\underline{n} = \underline{f}_d \quad \text{on } \partial_f\Omega & (4a) \\ \text{Dirichlet boundary conditions: } \underline{u} = \underline{u}_d \quad \text{on } \partial_u\Omega, & (4b) \end{cases}$$

where $\underline{f}_d$ denotes the traction applied on the boundary $\partial_f\Omega$, with $\underline{n}$ the outward unit normal vector, and $\underline{u}_d$ is the applied displacement on the border $\partial_u\Omega$. Besides, $\partial_u\Omega$ and $\partial_f\Omega$ are defined such that $\partial_u\Omega \cap \partial_f\Omega = \emptyset$, so as to support a well-posed set of boundary conditions.

Simulated displacement measurements, denoted by $\underline{\tilde{u}}$, are available in a non-zero subdomain, defined as $\Omega_m \subset \Omega$:

$$\underline{u} = \underline{\tilde{u}} \qquad \text{in } \Omega_{\text{m}}. \tag{5}$$

The synthetic measurements are obtained from a reference FE calculation and an added random error as detailed in section 2.1.2.

The vector $\underline{\widetilde{u}}$ containing displacement measurements is defined such that $\underline{\widetilde{u}} \in \mathbb{R}^{2\times n_{\text{meas}}}$ for a 2D problem, with n_{meas} the number of data points corresponding to a realistic regular data grid. Displacement measurements can be seen as the sum of a free-of-error term $\underline{\widetilde{u}}_0$ and a perturbation term $\delta\underline{\widetilde{u}}$, so that

$$\underline{\widetilde{u}} = \underline{\widetilde{u}}_0 + \delta\underline{\widetilde{u}}. \tag{6}$$

2.1.2. Finite element formulation and data construction. A perturbation term $\delta\underline{\widetilde{u}}$ is constructed on the data grid and added to the free-of-error displacement term. Only inner displacement measurements are perturbed, whereas the mixed boundary conditions are assumed to be well known and reliable.

To implement the identification problem numerically, the continuous problem (1), (4) is discretized by the finite element method (FEM) (Dhatt *et al* 2012). The displacement is thus described, thanks to the FE shape functions, and can be expressed as

$$\underline{u}(\underline{x}) = [\Phi(\underline{x})]\{U\}\ ,\ \forall \underline{x} \in \Omega,$$

where the matrix $[\Phi(\underline{x})]$ collects the FE shape functions and $\{U\}$ collects the degrees of freedom (dofs) associated with $\underline{u}$. Then, the discretization of the direct problem leads to a linear system that can be expressed in a matricial manner as

$$[K]\{U\} = \{F\}, \tag{7}$$

where $[K]$ denotes the global rigidity matrix and $\{F\}$ is the generalized load vector which incorporates the boundary conditions (4).

Since $\underline{\theta}$ consists of the Lamé coefficients, it can be noted that the stiffness matrix is linear with respect to $\underline{\theta}$:

$$[K] = \sum_{j=1}^{p} \theta_j [K_j^1], \tag{8}$$

where $[K_j^1]$ is the constant matrix $\frac{\partial[K]}{\partial\theta_j}$.

In the following, synthetic displacements $\underline{u}_0$ are based on the previous FE model with the reference elastic properties $\underline{\theta}_0$. The subscript 0 refers to exact reference quantities. $\underline{u}_0$ is described through the vector of the corresponding dofs, $\{U_0\}$, whose length is denoted by N_{dof}.

Since the data grid should be representative of a DIC data grid (regular with a typical size of about 200×200), the measurements should not be defined on the FE mesh. Hence, a projection of $\underline{u}_0$ from the FE mesh to the data grid is necessary and is performed, thanks to a transfer operator Π. The last is based on the FE shape functions and yields the values of the FE displacement field at the points of the data grid. The synthetic displacement measurements are finally collected in the vector $\{\widetilde{U}\}$ such that

$$\{\widetilde{U}\} = [\Pi]\{U_0\} + \{\delta\tilde{U}\} = \{\tilde{U}_0\} + \{\delta\tilde{U}\}, \tag{9}$$

where $\delta\tilde{U}$ is a vector corresponding to the error between the measurements and the FE model. It is usually made of three parts.

(i) A measurement random error term characterized by its covariance matrix $[C]$. In practical cases, such a covariance matrix depends on the DIC algorithm (Sutton

et al 2009) and can be determined experimentally. Later, a reasonable hypothesis for the representation of $\{\delta\tilde{U}\}$ is to take random perturbations of white noise type. Nevertheless, the study can be performed for any covariance matrix related to a DIC study.

(ii) A measurement systematic error term inherent to the DIC technique and the acquired images (Bornert *et al* 2009). Such an error is not taken into account in the following numerical study.

(iii) A model error, related to an improper choice of the FE model in practical cases. Here, it is chosen to use the same FE model for the creation of the measurements and for the identification step. Hence, the model error is not taken into account.

As a consequence, we propose to study the effect of filtering on the identification results in cases with a random error but no systematic error (neither from the measurement nor the model). It is considered that systematic error in the input data would lead to a bias in the identification results, with or without filtering, and that the filtering will mainly modify the identification errors associated with the measurement random error.

2.1.3. Identification problem. The identification problem consists in finding the constitutive parameters $\underline{\theta}$ by confronting the direct problem (1), (4) with the measurement data (5). It is addressed as an inverse problem (Bonnet and Constantinescu 2005).

The inverse method adopted in this study is a least-squares formulation where the solution $\underline{\theta}^{\text{opt}}$ of the identification problem is minimizing the discrepancy between simulated and measured data. Since it requires FE simulations, such an approach is usually known as a FEMU. Here, the cost function to be minimized only covers the displacement measurements. The discrete identification problem can be presented in a monolithic manner as

find $(\{U\}, \underline{\theta})$ minimizing:

$$\begin{cases} \mathcal{J}(\{U\}, \underline{\theta}) = \frac{1}{2}([\Pi]\{U\} - \{\tilde{U}\})^{\mathsf{T}}[B]([\Pi]\{U\} - \{\tilde{U}\}) & (10a) \\ \text{under the constraint: } [K(\underline{\theta})]\{U\} = \{F\}, & (10b) \end{cases}$$

where $\mathcal{J}$ is the cost function expressing the least-squares formulation gap between the measurement and model, and $[B]$ is a matrix related to the chosen norm of the cost function.

Solving problem (10) usually consists in minimizing $\mathcal{J}$ with respect to $\underline{\theta}$, where $\{U\}$ is estimated through (10*b*) and is thus not dealt with as a minimization under constraint. Nevertheless, we keep here the above monolithic form which allows a practical first-order development in section 3.1.

2.2. The diffuse approximation as a filtering method

The study of the filtering effect on the identification results is based on the use of the DA for filtering. Let us note that such a study can be performed for any other filtering tool since it is characterized in terms of error. The DA was first developed for solving partial differential equations (Nayroles *et al* 1991b, Prax *et al* 1996, Sadat and Prax 1996), and then applied to optimization problems (Breitkopf *et al* 2002, Nayroles 1994) and field transfer (Brancherie *et al* 2006, Villon *et al* 2002). It has recently been applied to strain field estimation from full-field displacement data in Avril *et al* (2008a). The latter was first developed for 2D space measurements and then applied to spacetime data in Feissel *et al* (2011).

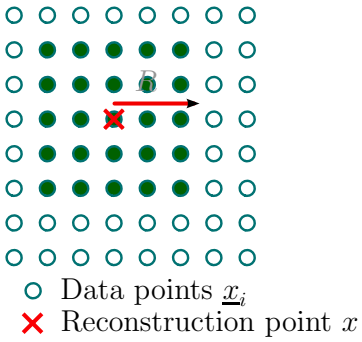

Figure 2. Reconstruction from the neighborhood of each point.

It consists in the reconstruction of a continuous field from a cloud of data points. In our context, the starting point is a displacement field obtained by a 2D-DIC technique, during a mechanical test.

The displacement is measured on a regular data grid, where $\underline{x}_i$ is the position of the ith data point and $\tilde{\underline{u}}(\underline{x}_i)$ the corresponding displacement data, $i \in [1, n_{\text{meas}}]$. $\tilde{\underline{u}}(\underline{x}_i)$ is described through its Cartesian coordinates $(\tilde{u}(\underline{x}_i), \tilde{v}(\underline{x}_i))$ associated with the directions of the data grid. For each coordinate $\tilde{u}$ and $\tilde{v}$, an approximated field is reconstructed as presented in the following for $\tilde{u}$. The approximated field is denoted as $u_{ap}(\underline{x})$ and is written as the product of a vector of coefficients $\underline{a}(\underline{x})$ and beforehand chosen shape functions, such that

$$u_{ap}(\underline{x}) = \underline{p}(\underline{x})\,\underline{a}(\underline{x}), \tag{11}$$

where $\underline{a}$ is to be determined and $\underline{p}(\underline{x})$ is a vector containing the functions of the approximation basis. The choice here is to use a degree 2 polynomial basis:

$$\underline{p}(\underline{x})^{\mathsf{T}} = \left\{1 \quad x \quad y \quad \frac{x^2}{2} \quad xy \quad \frac{y^2}{2}\right\}, \tag{12}$$

where x and y are respectively the horizontal and vertical Cartesian coordinates of the considered point. In each reconstruction point $\underline{x}$, $\underline{a}(\underline{x})$ is the solution of local-weighted least squares, defined on a neighborhood of $\underline{x}$, denoted as $V(\underline{x})$:

$$\min_{\underline{a}(\underline{x})} \frac{1}{2} \sum_{\underline{x}_i \in V(\underline{x})} w(\underline{x}, \underline{x}_i)(\underline{p}(\underline{x} - \underline{x}_i)^{\mathsf{T}}\underline{a}(\underline{x}) - \tilde{u}(\underline{x}_i))^2, \tag{13}$$

with $w(\underline{x}, \underline{x}_i)$ a weighting function with a local span implicitly defining $V(\underline{x})$:

$$w(\underline{x}, \underline{x}_i) = w_{\text{ref}}\left(\frac{x - x_i}{R_x}\right) w_{\text{ref}}\left(\frac{y - y_i}{R_y}\right). \tag{14}$$

w_{ref} refers to a third-order spline approximating a Gaussian function but with a local span in $[-1,\ 1]$.

R_x and R_y are the radii at each reconstruction point $\underline{x}$, in the x and y directions, as illustrated in figure 2. In the following, we will consider $R_x = R_y = R$ constant all over the data grid. R

constitutes a main parameter allowing the adjustment between the approximation error and the random error as detailed in section 2.3.

In a matricial form, equation (13) can be written at any $\underline{x}$ as

$$\min_{\{a\}} \tfrac{1}{2}[[P]\{a\} - \{\tilde{U}_{\underline{x}}\}]^{\mathsf{T}}[W][[P]\{a\} - \{\tilde{U}_{\underline{x}}\}], \tag{15}$$

where $[W]$ is a diagonal matrix made up of the weighting functions $w(\underline{x}, \underline{x}_i)$, $[P]$ is a matrix made up of $\underline{p}(\underline{x} - \underline{x}_i)$ lines and $\{\tilde{U}_{\underline{x}}\}$ is a vector containing the data corresponding to the points in $V(\underline{x})$.

We deduce the linear system satisfied by the solution $\{a\}$ of equation (15), which is written as

$$\{a\} = [P^{\mathsf{T}}WP]^{-1}[P]^{\mathsf{T}}[W]\{\tilde{U}\}. \tag{16}$$

If the projection basis is of degree 1 or more, the reconstructed field and its first derivatives in a diffuse manner at point $\underline{x}$ are given by the first three components of the vector $\{a\}$:

$$a_1(\underline{x}) = u_{ap}(\underline{x}); \quad a_2(\underline{x}) = \frac{\delta u_{ap}}{\delta x}(\underline{x}); \quad a_3(\underline{x}) = \frac{\delta u_{ap}}{\delta y}(\underline{x}),$$

where $\frac{\delta u_{ap}}{\delta x}$ and $\frac{\delta u_{ap}}{\delta y}$ are the *diffuse* first derivatives referring to an estimation of the exact derivatives. We choose to perform a reconstruction for each data point of the measured field $\tilde{\underline{u}}$. Hence, we should solve problem (15) at each data point. The reconstruction is performed for the two components of $\tilde{\underline{u}}$ and the discrete reconstructed field is collected in $\{U_{ap}\}$.

Let us underline that the presented approximation approach is linear and $\{U_{ap}\}$ is obtained by applying a reconstruction matrix $[M_u]$ on a given measured displacement vector $\{\tilde{U}\}$:

$$\{U_{ap}\} = [M_u]\{\tilde{U}\}. \tag{17}$$

$[M_u]$ is made up from the lines of (16) corresponding to the first coefficient a_1 of the reconstruction points taken into account. In our case, it is a ($2\ n_{\text{meas}} \times 2\ n_{\text{meas}}$) matrix when considering the global reconstruction operator. Moreover, if the reconstructed strain field $\{\epsilon_{ap}\}$ is needed, we can deduce them subsequently from the first-order diffuse derivatives, leading to a similar reconstruction operator:

$$\{\epsilon_{ap}\} = [M_\epsilon]\{\tilde{U}\}, \tag{18}$$

where $[M_\epsilon]$ denotes the reconstruction matrix of strains and is deduced from the lines of (16) associated with a_2 and a_3.

In summary, the parameters controlling the diffuse reconstruction are the degree of the projection basis and the radius R of the weighting function. The next section describes the errors when reconstructing a displacement field $\{\tilde{U}\}$ using the DA method.

2.3. Approximation error and random error

Considering a displacement described as the sum of an exact displacement and random measurement perturbations (6), the reconstructed displacement field $\underline{u}_{ap}$ at each point $\underline{x}_i$ is written as

$$\underline{u}_{ap}(\underline{x}_i) = \underline{u}_0(\underline{x}_i) + \underbrace{\delta\underline{u}_k(\underline{x}_i)}_{\text{approximation error}} + \underbrace{\delta\underline{u}_b(\underline{x}_i)}_{\text{random error}}, \tag{19}$$

where

- $\underline{u}_0$ is the exact field.
- $\delta\underline{u}_k$ is the approximation error and is associated with the reconstruction of the exact field. It is related to the loss of mechanical information.
- $\delta\underline{u}_b$ is the random error on the reconstructed field characterized from the reconstruction of measurement perturbations alone.

As the span R is increased, the random error is reduced but the approximation error is increased. There is a trade-off to be found for the choice of R, aiming at reducing the random error while maintaining an acceptable level for the approximation error. Due to the linearity of the reconstruction, the two types of errors can be studied separately. In fact, this decomposition cannot be done on a real case since the exact field remains unknown, but it allows us to characterize the displacement reconstruction from a theoretical point of view.

It can be shown that the approximation error is related to the $n+1$ Taylor remainder of the exact field, when dealing with a polynomial basis of degree n (Feissel 2012). An error estimator for the Taylor remainder is necessary to characterize it but is still to be developed. On the other hand, the random error is directly linked to the raw field perturbations, denoted by $\{\delta\tilde{U}\}$, through the reconstruction matrix $[M_u]$:

$$\{\delta U_b\} = [M_u]\{\delta\tilde{U}\}. \tag{20}$$

When measurement perturbations can be described from a statistical point of view, so can be the random error.

Measurement random error is usually characterized through a covariance matrix $[C]$ as mentioned in section 2.1.1. Its expression is written as

$$[C] = \langle\{\delta\tilde{U}\}\{\delta\tilde{U}\}^{\mathsf{T}}\rangle = {\sigma_b}^2[C_0], \tag{21}$$

where the notation $\langle\ \rangle$ corresponds to the expectation, σ_b is the standard deviation describing the random error magnitude and $[C_0]$ is the spatial correlation matrix. Such information can be known from the chosen 2D-DIC algorithm (e.g. CORRELI^{Q4} (Hild and Roux 2006)).

From (20), the covariance of $\{\delta U_b\}$ can easily be estimated:

$$\text{Cov}(\{\delta U_b\}) = {\sigma_b}^2[M_u][C_0][M_u]^{\mathsf{T}}. \tag{22}$$

In the following, we will characterize the link between these errors and the induced identification error from a FEMU approach, so that we can discuss the suitability of filtering for the identification purpose.

3. Theoretical study of the identification error

3.1. Identification problem

In order to characterize the effects of filtering on the identification results, we propose to characterize analytically the relationship between the identification error and the measurement perturbations from a first-order analysis. Such a first-order study can be performed in several ways. The sensitivity matrix is computed analytically, using the EGM in Amiot *et al* (2006) and the FEMU approach in Gras *et al* (2012). Here, we choose to base our study on a perturbation

analysis of the optimality problem associated with (10). Such an approach, within the framework of adjoint problems, remains general and could allow us to perform the study for nonlinear problems. To that purpose, let us start from the identification problem (10).

To solve it, a Lagrangian is introduced:

$$\mathcal{L} = J(\{U\}, \underline{\theta}) - \{\Lambda\}^{\mathsf{T}}([K(\underline{\theta})]\{U\} - \{F\}). \tag{23}$$

Then, the Lagrangian stationarity $\left(\frac{\partial \mathcal{L}}{\partial \Lambda}, \frac{\partial \mathcal{L}}{\partial U}, \frac{\partial \mathcal{L}}{\partial \theta}\right) = (0, 0, 0)$ leads to the following optimality system with respect to $(\{U\}, \{\Lambda\}, \underline{\theta})$:

$$\begin{cases} [K]\{U\} = \{F\} & (24a) \\ [K]^{\mathsf{T}}\{\Lambda\} = [\Pi]^{\mathsf{T}}([B]([\Pi]\{U\} - \{\tilde{U}\})) & (24b) \\ \{\Lambda\}^{\mathsf{T}}\left[K_j^1\right]\{U\} = \{0\}, \qquad \forall j \in [1, p]. & (24c) \end{cases}$$

In order to set up the relationship between the identification error and measurement perturbations, a first-order analysis of the perturbation of the solution of (24) with respect to a perturbation on the measurements is performed as detailed in section 3.2.

3.2. First-order analysis

For a set of perturbed measurements, the identification error, denoted by $\{\delta\theta\}$, is defined as the difference between the p identified material properties and the reference values (free-of-error).

The starting point consists in seeking the relationship between the identification error $\{\delta\theta\}$ and the measurement perturbations $\{\delta\tilde{U}\}$ based on a first-order approximation. A sensitivity matrix is thus introduced:

$$\{\delta\theta\} = [S^\theta]\{\delta\tilde{U}\} + o(\{\delta\tilde{U}\}). \tag{25}$$

In order to determine the sensitivity matrix $[S^\theta]$, we propose here to construct it column by column. Each column is determined via solving problem (24) at the first order, by perturbing successively each component of $\{\tilde{U}\}$. Let us therefore introduce the pinpoint perturbation $\delta\tilde{u}$, defined as

$$\{\delta\tilde{U}\} = \delta\tilde{u}\{e_i\}, \qquad \forall i \in [1, 2n_{\text{meas}}], \tag{26}$$

where the index i denotes the considered measurement degree of freedom, $2n_{\text{meas}}$ is the total number of measurement dofs for a 2D problem and $\{e_i\}$ is a unit vector defined as $e_i(l) = \delta_{li}$, with δ_{li} the *Kronecker* delta. Therefore, for such a defined perturbation, the first-order development of the identification error with respect to $\delta\tilde{u}$ is written as

$$\{\delta\theta\} = \{S^\theta_{.i}\}\delta\tilde{u} + o(\delta\tilde{u}), \qquad \forall i \in [1, 2n_{\text{meas}}], \tag{27}$$

where $\{S^\theta_{.i}\} = [S^\theta]\{e_i\}$ is a $p \times 1$ vector and corresponds to the ith column of the sought sensitivity matrix $[S^\theta]$.

In the same manner, sensitivity matrices are introduced for $\{U\}$ and $\{\Lambda\}$:

$$\begin{cases} \{U\} = \{U_0\} + \{S^u_{.i}\}\delta\tilde{u} + o(\delta\tilde{u}) & (28a) \\ \{\Lambda\} = \{\Lambda_0\} + \{S^\Lambda_{.i}\}\delta\tilde{u} + o(\delta\tilde{u}), & (28b) \end{cases}$$

where $\left\{S^u_{.i}\right\}$ and $\left\{S^\Lambda_{.i}\right\}$ have N_{dof} lines denoting the total number of FE dofs.

From equations (8) and (27), the first-order writing of the symmetric global rigidity matrix takes the following form:

$$[K(\underline{\theta})] = \underbrace{[K(\underline{\theta}_0)]}_{\stackrel{=}{\text{def}}[K_0]} + \sum_{j=1}^{p}\left[K_j^1\right]S^\theta_{ji}\delta\tilde{u} + o(\delta\tilde{u}). \tag{29}$$

Now, let us make a first-order development of the optimality system (24) by taking into account the development with respect to $\delta\tilde{u}$ and partitioning each equation in order 0 and order 1, neglecting higher order terms. From equations (28a) and (29), (24a) is written as

$$\begin{cases} [K_0]\{U_0\} = \{F\} & (30a) \\ [K_0]\{S^u_{.i}\} + \sum_{j=1}^{p}[K_j^1]S^\theta_{ji}\{U_0\} = \{0\}. & (30b) \end{cases}$$

Using equations (28) and (29), (24b) becomes

$$\begin{cases} [K_0]^{\mathsf{T}}\{\Lambda_0\} = [\Pi]^{\mathsf{T}}[B]\underbrace{([\Pi]\{U_0\} - \{\tilde{U}_0\})}_{=\{0\}} = \{0\} & (31a) \\ [K_0]^{\mathsf{T}}\{S^\Lambda_{.i}\} + \left(\sum_{j=1}^{p}\left[K_j^1\right]S^\theta_{ji}\right)^{\mathsf{T}}\{\Lambda_0\} \\ \quad = [\Pi]^{\mathsf{T}}[B]([\Pi]\{S^u_{.i}\} - \{e_i\}), & (31b) \end{cases}$$

where the free-of-error measured term $\{\tilde{U}_0\}$ is assumed to be equal to the projection of the reference displacement vector on the data grid (9).

In the same way, equation (24c) takes the following form:

$$\begin{cases} \{\Lambda_0\}^{\mathsf{T}}\left[K_j^1\right]\{U_0\} = \{0\}, \qquad \forall j \in [1, p] & (32a) \\ \{S^\Lambda_{.i}\}^{\mathsf{T}}\left[K_j^1\right]\{U_0\} + \{\Lambda_0\}^{\mathsf{T}}\left[K_j^1\right]\{S^u_{.i}\} = \{0\}, \qquad \forall j \in [1, p]. & (32b) \end{cases}$$

Bringing together the zero-order equations (30a), (31a) and (32a) leads to

$$\begin{cases} \{U_0\} = [K_0]^{-1}\{F\} & (33a) \\ \{\Lambda_0\} = \{0\}. & (33b) \end{cases}$$

The zero-order equations correspond to the optimality problem for the exact measurements, with the reference parameters $\underline{\theta} = \underline{\theta}_0$, leading to (33$b$).

By using equations (30b), (31b), (32b) and (33b), one obtains the following order 1 system:

$$\begin{cases} \{S^u_{.i}\} = -[K_0]^{-1}\sum_{j=1}^{p}\left[K_j^1\right]\{U_0\}S^\theta_{ji} & (34a) \\ \{S^\Lambda_{.i}\} = [K_0]^{-1}[\Pi]^{\mathsf{T}}[B]([\Pi]\{S^u_{.i}\} - \{e_i\}) & (34b) \\ \{S^\Lambda_{.i}\}^{\mathsf{T}}\left[K_j^1\right]\{U_0\} = \{0\} \qquad \forall j \in [1, p]. & (34c) \end{cases}$$

By introducing

$$\begin{cases} \left\{U_j^1\right\} = [K_0]^{-1}\left[K_j^1\right]\{U_0\} & (35a) \\ \left[U_m^1\right] = \left[\left\{U_1^1\right\}, \ldots, \left\{U_p^1\right\}\right], & (35b) \end{cases}$$

equation (34a) can be expressed as

$$\{S^u_{.i}\} = -\sum_{j=1}^{p} \{U^1_j\} S^\theta_{ji} = -[U^1_m] S^\theta_{.i}. \tag{36}$$

We then obtain the following linear system on $\{S^\theta_{.i}\}$:

$$[U^1_m]^\mathsf{T}[\Pi]^\mathsf{T}[B][\Pi][U^1_m]\{S^\theta_{.i}\} = -[U^1_m]^\mathsf{T}[\Pi]^\mathsf{T}[B]\{e_i\}, \quad \forall i \in [1, 2n_{\text{meas}}]. \tag{37}$$

Thus, solving the system (34) for $\{\delta\tilde{U}\} = \delta\tilde{u}\{e_i\}$ yields the equation satisfied by the ith column of the sought sensitivity matrix. Taking into account these equations for all i, $[S^\theta]$ is obtained as

$$[S^\theta] = -\left([U^1_m]^\mathsf{T}[\Pi]^\mathsf{T}[B][\Pi][U^1_m]\right)^{-1}[U^1_m]^\mathsf{T}[\Pi]^\mathsf{T}[B]. \tag{38}$$

In summary, the sensitivity matrix yields the first-order relation between measurement perturbations and the identification error.

3.3. Characterizing the identification errors—bias and variance

The aim of this theoretical study is to discuss and compare the robustness of the identification results with and without filtering on a numerical example. The definition of an enhancement criterion is thus necessary. A criterion based on the calculation of the bias and the variance of the identification error without and with a filtering step is set up.

Let us write the first-order analytical expressions of both bias and variance of the identification error $\{\delta\theta\}$ using the previous developments.

Let us also consider a given measurement perturbation vector $\{\delta U\}$. From relationship (25), both the bias and the covariance are expressed at the first order as follows:

- Bias of $\{\delta\theta\}$:

$$\langle\{\delta\theta\}\rangle = [S^\theta]\langle\{\delta U\}\rangle \tag{39}$$

- Covariance of $\{\delta\theta\}$:

$$\begin{aligned}\text{Cov}(\{\delta\theta\}) &= \langle(\{\delta\theta\} - \langle\{\delta\theta\}\rangle)^2\rangle \\ &= [S^\theta]\,\text{Cov}(\{\delta U\})[S^\theta]^\mathsf{T}.\end{aligned} \tag{40}$$

The quality of the identification is assessed by computing the standard deviation and the bias of the identification error for two types of displacement data measurements for the inverse problem.

(1) Raw field $\{\tilde{U}\}$ (without filtering).
The measurement field is constructed using a reference FE simulation, and mixed with artificial perturbations, as described in section 2.1.2. In the following, the latter are created from a Gaussian white noise characterized by a zero mean and a given standard deviation σ_b summed up as

$$\{\delta U\} \sim \mathcal{N}(0, {\sigma_b}^2[Id]), \tag{41}$$

where $[Id]$ is the identity matrix.

(a) Mean of the identification error $\langle\{\delta\theta\}\rangle_{\text{raw}}$.
Since measurement perturbations are centered, the mean of the identification error is equal to zero:

$$\langle\{\delta\theta\}\rangle_{\text{raw}} = \{0\}. \tag{42}$$

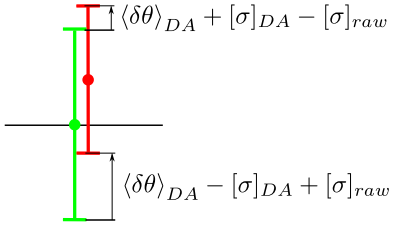

Figure 3. Enhancement criterion for the filtering assessment.

Table 1. Expression of the bias and the covariance for two types of data.

	Without filtering	With filtering
$\langle\{\delta\theta\}\rangle$	$\{0\}$	$[S^\theta]\delta U_k$
$\text{Cov}(\{\delta\theta\})$	${\sigma_b}^2([S^\theta {S^\theta}^\mathsf{T}])$	${\sigma_b}^2([S^\theta M_u {M_u}^\mathsf{T} {S^\theta}^\mathsf{T}])$

(b) Covariance of the identification error $\text{Cov}(\{\delta\theta\})_{\text{raw}}$.
Using equation (40), the covariance of the identification error is written as

$$\begin{aligned}\text{Cov}(\{\delta\theta\})_{\text{raw}} &= [S^\theta]\langle\{\delta U\}\{\delta U\}^\mathsf{T}\rangle[S^\theta]^\mathsf{T} \\ &= {\sigma_b}^2([S^\theta][S^\theta]^\mathsf{T}).\end{aligned} \tag{43}$$

(2) Reconstructed field $\{U_{ap}\}$ (with filtering).
The second measurement type is the approximated field reconstructed from the raw field by the DA. According to section 2.3, we dispose of both approximation and random errors after the reconstruction step, when dealing with a numerical example. Thus, the error in the reconstructed field is characterized by a mean value corresponding to the approximation error δU_k and the covariance of the random error (41):

$$\begin{aligned}\{\delta U_{ap}\} &= \underbrace{\{\delta U_k\}}_{\text{approximation error}} + \underbrace{\{\delta U_b\}}_{\text{random error}} \\ &\sim \mathcal{N}(\delta U_k, {\sigma_b}^2[M_u][M_u]^\mathsf{T}).\end{aligned} \tag{44}$$

(a) Mean of the identification error $\langle\{\delta\theta\}\rangle_{\text{DA}}$.
Due to the approximation error, we are saddled with a non-zero mean of the identification error:

$$\langle\{\delta\theta\}\rangle_{\text{DA}} = [S^\theta]\,\delta U_k. \tag{45}$$

(b) Covariance of the identification error $\text{Cov}(\{\delta\theta\})_{\text{DA}}$.
The covariance is calculated in the same way as previously, so that

$$\begin{aligned}\text{Cov}(\{\delta\theta\})_{\text{DA}} &= [S^\theta]\langle\{\delta U_b\}\{\delta U_b\}^\mathsf{T}\rangle[S^\theta]^\mathsf{T} \\ &= {\sigma_b}^2([S^\theta][M_u][M_u]^\mathsf{T}[S^\theta]^\mathsf{T}).\end{aligned} \tag{46}$$

In the end, the proposed analysis boils down to the calculation of the bias and the covariance of the identification error with and without DA filtering. Its recap is given in table 1.

In order to compare the identification results with and without filtering, an enhancement criterion is proposed for each parameter θ_j. Filtering improves the identification if the error bar of the identification with filtering is included in the one without filtering. This implies

$$\begin{cases}\langle\delta\theta_j\rangle_{\text{DA}} + (\sigma_{jj})_{\text{DA}} - (\sigma_{jj})_{\text{raw}} < 0 & (47a)\\ \langle\delta\theta_j\rangle_{\text{DA}} - (\sigma_{jj})_{\text{DA}} + (\sigma_{jj})_{\text{raw}} > 0, & (47b)\end{cases}$$

with $\sigma_{jj} = \text{Cov}\,(\{\delta\theta\})_{jj}$. The criterion is illustrated in figure 3.

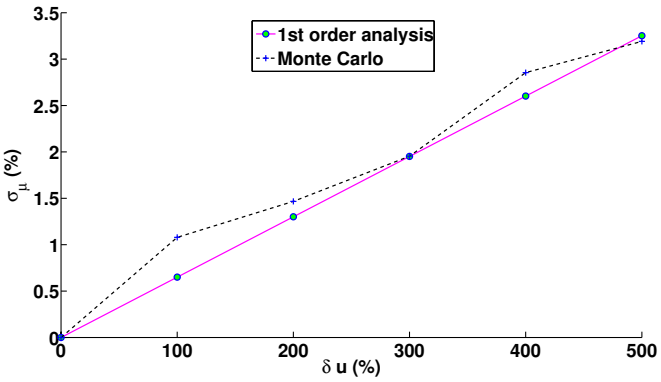

Figure 4. Standard deviation as a function of the synthetic perturbation level.

3.4. Validation of the theoretical analysis

In order to validate the proposed first-order analysis, it is compared to a Monte Carlo approach where 1000 identifications were performed from 1000 random samplings of Gaussian white noise added to the exact measurements.

The corresponding case test consists of a homogeneous square plate clamped in the load direction on its left-hand side and subjected to parabolic traction on the opposite side.

For the sake of simplicity, only a homogeneous μ is sought while λ is assumed to be known. A 100×100 measurement grid is constructed and the identification is performed within the framework detailed in section 2.1. Such an inverse problem with reliable boundary conditions is robust to measurement perturbations, due to the perturbations averaging on the whole domain during the identification process.

In order to significantly affect data, the prescribed perturbation levels reach 500% of the mean value of the displacement field.

Figure 4 shows the standard deviation of the identification error of μ as a function of the displacement perturbations for both analytic and Monte Carlo approaches. It can be seen that the first-order results fit well the Monte Carlo results, which validates the proposed approach.

It is then possible to proceed to the study of the effect of the DA filtering and the choice of an adequate least-squares norm on the identification results.

4. Effects of filtering on the identification results

In this section, the first-order analysis proposed in section 3.2 is applied to the identification of elastic properties from synthetic data, coupling the FEMU approach (section 2.1.3) with the DA filtering (section 2.2). The corresponding numerical test involves non-uniform strain fields in the studied region, and heterogeneous properties are sought.

4.1. Data construction and identification framework

The application concerns the example of a square plate with a centered inclusion. The displacement measurements are created through a reference calculation, using the FEM under the hypothesis of plane stress, where the mesh elements are triangles with linear shape functions. The plate is composed of two homogeneous isotropic elastic materials (the inclusion and its outside) with stiffer values for the inclusion properties. The stiffness tensor is written as a function of the Lamé coefficients λ and μ.

The measurement grid size is 100×100, and Gaussian white noise with a realistic 5% standard deviation is added in order to represent the measurement random error. Figure 5 shows the stress fields σ_{xx} and σ_{yy} generated by the simulation of a line traction on both right and left sides of the plate, illustrating the large stress gradients near the inclusion.

We choose to limit the identification to the μ parameter, outside the inclusion, which is assumed to be a piecewise constant. Hence, the λ parameter outside the inclusion and the stiffness of the inclusion are assumed to be known, which remains valid for the comparison purpose of the study. Thereby, the sought vector of parameters $\underline{\theta}$ contains the μ coefficients corresponding to the piecewise constant zones and its size is equal to the number of constant zones in the plate. The number of constant zones is a parameter of the inverse problem. The more it increases, the more ill-posed the inverse problem is.

As presented in section 2.1.3, the identification is based on the FEMU method and consists in the minimization of the quadratic gap between the measurements and the simulated data. It implies the choice of an associated norm by defining the weighting matrix $[B]$ in $(10a)$. Such a choice impacts the identification error (table 1) through the sensitivity matrix (38). It represents a second inverse problem parameter to be

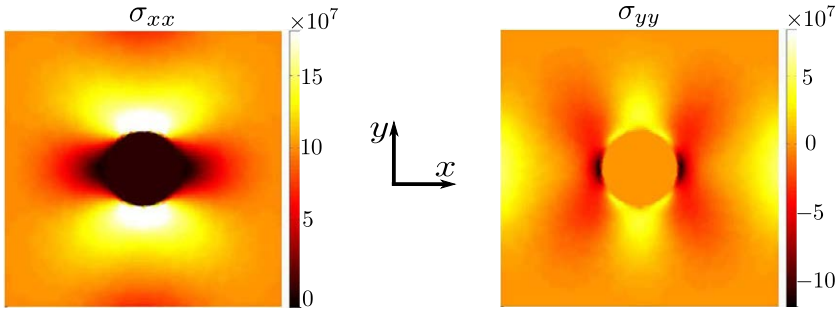

Figure 5. σ_{xx} and σ_{yy} stress maps of the tensile simulation.

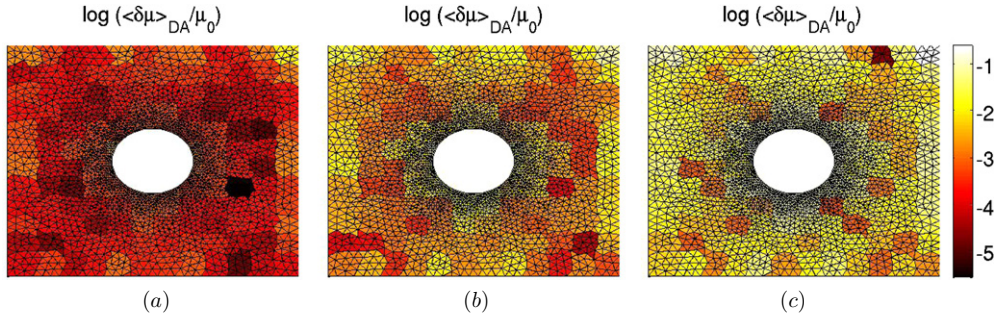

Figure 6. Bias maps for different spans: (*a*) $R = 3$, (*b*) $R = 6$ and (*c*) $R = 10$.

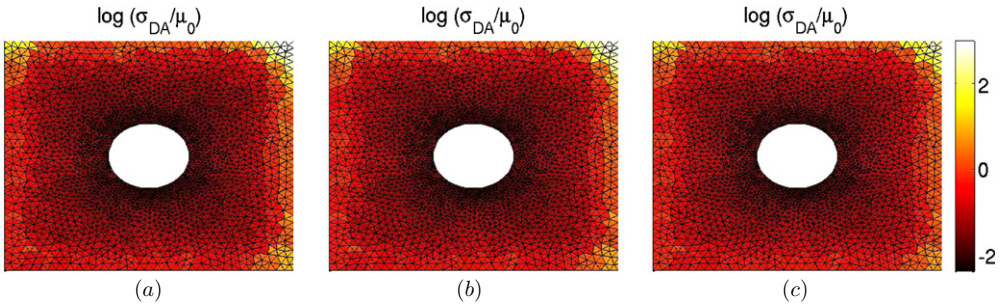

Figure 7. Standard deviation for different spans: (*a*) $R = 3$, (*b*) $R = 6$ and (*c*) $R = 10$.

studied. First, $[B]$ is chosen equal to the identity matrix, so that equation (10*a*) is written as

$$J(\{U\}, \underline{\theta}) = \tfrac{1}{2}([\Pi]\{U\} - \{\tilde{U}\})^{\mathsf{T}}([\Pi]\{U\} - \{\tilde{U}\}). \qquad (48)$$

The results are compared, based on the bias and the standard deviation of the identification error for both raw and reconstructed measurements. Then, the enhancement criterion developed in section 3.3 is studied. Since we choose to perform the identification in a heterogeneous way, all these quantities are calculated for each constant zone.

4.2. Influence of the problem parameters

4.2.1. Effect of the filtering span. The effect of filtering on the identification results is studied by considering the DA tool presented in section 2.2. The filtering parameter is the span R defining the physical size of the neighborhood for each reconstruction point (14) and is chosen constant all over the measurement zone.

Figure 6 shows three maps of the logarithm of the bias on the identification $\langle\{\delta\mu\}\rangle_{\mathrm{DA}}$, normalized by the reference values of μ, for three different filtering spans. As expected, the bias increases with the span because of the approximation error (45).

Figure 7 shows three maps of the standard deviation computed for three different spans, and points out that the larger the span the lower the variance, because of averaging of the random error on a larger area. Furthermore, the standard deviation is larger at the edges of the plate, due to an increasing error from the DA (Feissel 2012). It can be noted that the area with larger bias corresponds to the area near the inclusion, where the large gradient of the strain field implies a large approximation error by the DA. The effect of such an error on the displacement field implies an error in the identified parameters that remains local. At the end, an adequate span reflects a trade-off between the bias and the standard deviation.

4.2.2. Effect of the size of the constant zones. The size of the constant zones is an important parameter of the inverse problem. As the constant zones become smaller, the number of unknown parameters increases leading to a more difficult identification. The μ parameter of a given constant zone is actually impacting the displacement field in the vicinity of the considered zone which decreases with the size of the zone, hence increasing the effect of measurement perturbations. There is thus a limit to the spatial resolution that can be expected. This is confirmed by the proposed approach, which shows that the magnitudes of both the bias and the standard deviation of the identification error increase as the size of the constant zones decreases. Figure 8 shows the standard deviation of the identification error for three different sizes of constant zones in the case of raw data.

4.2.3. Identification enhancement. In this section, we discuss the effect of filtering on the identification results in more detail. As mentioned previously, there is a trade-off to be found between the bias and the standard deviation to choose the proper span R. The trade-off depends at least on the size of the constant zones, the measurement perturbation level and the local strain gradients. The measurement perturbation level is fixed to a 5% magnitude, representative of an experimental random error when dealing with specimens in the elastic range. The effect of the local strain gradients is illustrated in figure 9, where the identification results are plotted for three different constant zones: on the border, near the inclusion and in a middle zone. In each subfigure, the two border lines define the error bar of the identification without filtering, from

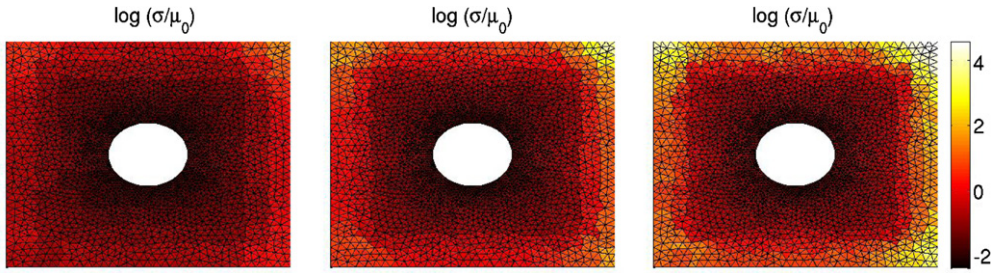

(a) (b) (c)

Figure 8. Standard deviation for different sizes of constant zones (without filtering): (*a*) large size, (*b*) middle size and (*c*) small size.

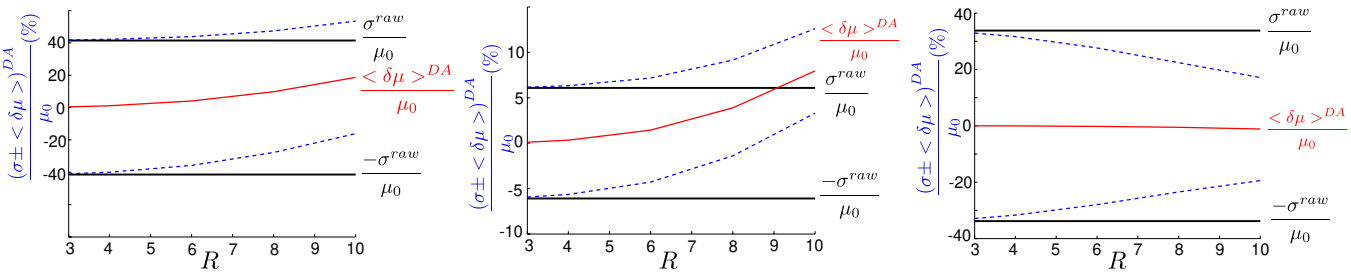

(a) (b) (c) middle zone

Figure 9. Local identification error as a function of the filtering span: (*a*) border zone, (*b*) zone near the inclusion and (*c*) middle zone.

the standard deviation of the identification error. The middle continuous line represents the bias of the identification error with filtering, while the dashed lines represent the error bar around the bias with filtering. All these quantities are here normalized by the reference value of the Lamé constant μ_0.

In the case of figures 9(*a*) and (*b*), the bias is dominating whatever the span R is; hence, the filtering does not enhance the identification. Figure 9(*c*) indicates the enhancement of the identification with filtering all the more when R becomes larger. From these local results, it is possible to apply the criterion (47) for each constant zone, leading to enhancement maps, as illustrated in figure 10. The color key is defined via a linear color gradient specified by the values 1 and -1, such that light colors correspond to an enhancement zone, while dark colors represent a non-enhancement zone.

The following trends can be observed on the proposed example.

The filtering improves the identification results all the more when the size of the constant zones is small. For large constant zones, filtering should not be necessary. Nonetheless, the identification is not improved by the filtering in the vicinity of the inclusion, because of large strain gradients in this area. The best results can be observed in figure 10(*c*) corresponding to a span R of 4. However, in spite of an obvious improvement of the identification by filtering, let us note that the identification is globally rather inaccurate when looking at the average error level with or without filtering in the studied example (figure 9), where the limit of affordable spatial resolution is reached.

4.3. Choice of the identification norm

In the following section, we study how the choice of the norm for the least-squares formulation (10*a*) affects the identification results. As mentioned in section 4.1, the previous results correspond to the basic choice of an identity matrix as a weighting matrix of the cost function. For filtered data, such a choice leads to a non-zero bias of the identification error.

In order to avoid the identification bias, while keeping the filtering step, we propose to include it within the identification step by modifying the weighting matrix $[B]$. Two additional norms are therefore tested.

(i) Filtered displacement norm: by filtering both measured and calculated fields, we get the same approximation error for the two reconstructed fields. The discrepancy between the two fields thus becomes free of the approximation error, yielding a zero bias (45). The cost function (10*a*) reads

$$J(\{U\},\underline{\theta}) = \tfrac{1}{2}([\Pi]\{U\} - \{\tilde{U}\})^{\mathsf{T}}[M_u]^{\mathsf{T}}[M_u]([\Pi]\{U\} - \{\tilde{U}\}) \qquad (49)$$

with $[B] = [M_u]^{\mathsf{T}}[M_u]$.
The sensitivity matrix (38) takes the following form:

$$[S^\theta] = \left(\left[U_m^1\right]^{\mathsf{T}}[\Pi]^{\mathsf{T}}[M_u]^{\mathsf{T}}[M_u][\Pi]\left[U_m^1\right]\right)^{-1} \times \left[U_m^1\right]^{\mathsf{T}}[\Pi]^{\mathsf{T}}[M_u]^{\mathsf{T}}[M_u]. \qquad (50)$$

(ii) Filtered strain norm: alternatively, the cost function can be based on the strain fields, considering the sensitivity of the strain fields to the material properties, disregarding their inescapable sensitivity to the measurement perturbations. The only modification to the approach is to replace the displacement operator $[M_u]$ by the strain operator $[M_\epsilon]$. The cost function of the identification problem becomes

$$J(\{U\},\underline{\theta}) = \tfrac{1}{2}([\Pi]\{U\} - \{\tilde{U}\})^{\mathsf{T}}[M_\epsilon]^{\mathsf{T}}[M_\epsilon] \times ([\Pi]\{U\} - \{\tilde{U}\}) \qquad (51)$$

with $[B] = [M_\epsilon]^{\mathsf{T}}[M_\epsilon]$.

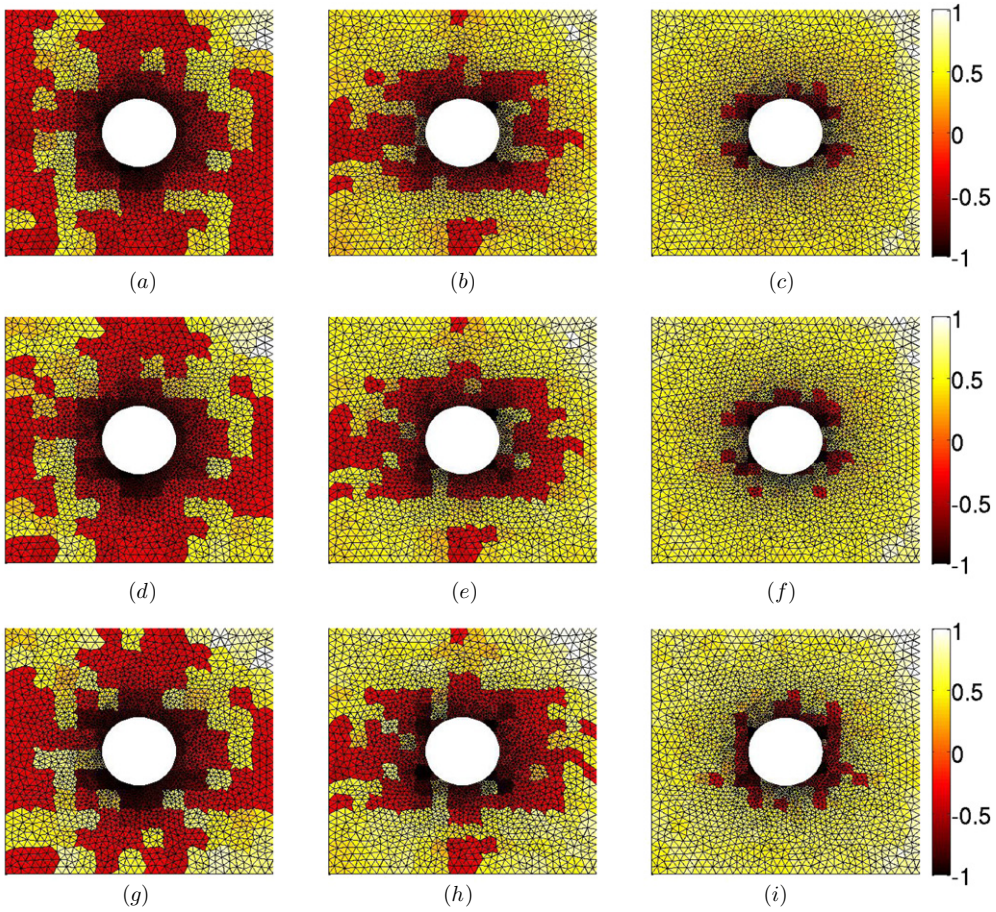

Figure 10. Enhancement maps for various spans and zone sizes: (*a*) large size ($R = 4$), (*b*) middle size ($R = 4$), (*c*) small size ($R = 4$), (*d*) large size ($R = 6$), (*e*) middle size ($R = 6$), (*f*) small size ($R = 6$), (*g*) large size ($R = 10$), (*h*) middle size ($R = 10$) and (*i*) small size ($R = 10$).

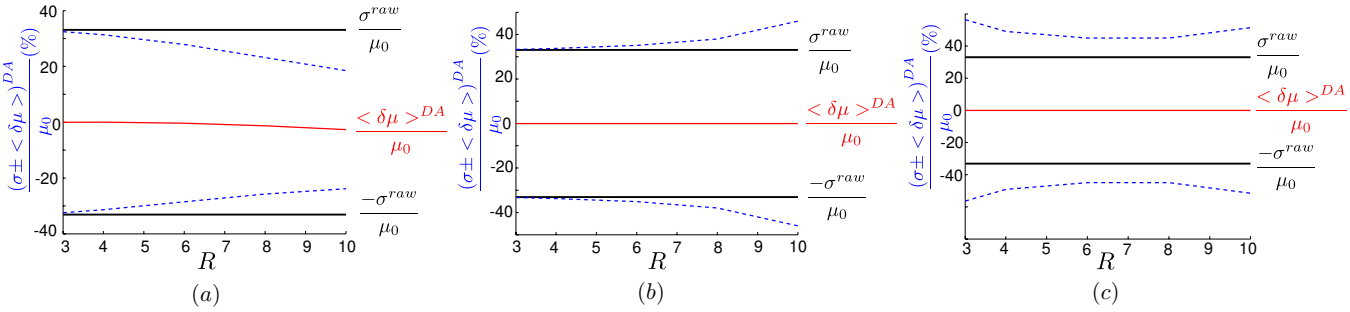

Figure 11. Local identification error for different cost function norms: (*a*) $[B] = [Id]$, (*b*) $[B] = [M_u]^{\mathsf{T}}[M_u]$ and (*c*) $[B] = [M_\epsilon]^{\mathsf{T}}[M_\epsilon]$.

The sensitivity matrix (38) takes the following form:

$$[S^\theta] = \left(\left[U_m^1\right]^{\mathsf{T}}[\Pi]^{\mathsf{T}}[M_\epsilon]^{\mathsf{T}}[M_\epsilon][\Pi]\left[U_m^1\right]\right)^{-1} \times \left[U_m^1\right]^{\mathsf{T}}[\Pi]^{\mathsf{T}}[M_\epsilon]^{\mathsf{T}}[M_\epsilon]. \quad (52)$$

Figure 11 presents the local evolution of both bias and standard deviation of the identification error as a function of the filtering span, for a given constant zone. For each norm, the two border lines delimit the error bar of identification without filtering, where $[B] = [Id]$. The middle continuous line represents the bias of the identification error with filtering and the dashed lines represent the error bar of the identification with filtering.

It appears that, in spite of avoiding the bias on the identification, the new tested norms do not improve the identification since they increase the standard deviation. An increase of the filtering span emphasizes this phenomenon. This can be understood from the fact the filtering blurs both data and calculation fields, leading to a loss of mechanical information and a decrease of the sensitivity of the fields with respect to the material parameters. As a consequence, the gain associated with the loss of bias is compensated by the loss associated with the increase of the standard deviation, so that the alternative norms are not relevant on the studied example. Let us note that the illustrated deterioration between the norms is observed all over the plate.

5. Conclusion

This paper presented a study of the effect of the DA filtering on identification results based on the FEMU approach. The emphasis was to discuss the efficiency of a non-mechanical filter in the presence of a measurement random error. To this end, the relationship between measurement perturbations and the identification error was characterized through a first-order analysis.

The methodology was then applied to a numerical example where heterogeneous elastic properties were sought. The identification results with filtered measurements are satisfactory on the studied example, in comparison to the use of raw measurements. More precisely, it was shown that filtering was more effective when the zones with constant parameters were smaller. Furthermore, it was observed that the identification results were deteriorated by filtering in the areas with large strain gradients.

Besides, studying the choice of the cost function norm led to the conclusion that using displacements rather than strains was more accurate and that the filtering of the simulated data was not improving the identification results.

The proposed methodology can be applied in a study that precedes experimental identification: considering the numerical modeling of the experiment and taking into account a realistic random error, the tuning of filtering can be studied beforehand in order to estimate the expected accuracy and spatial resolution of the identification results. Then, it could be used after the identification from real test data as a tool to estimate the uncertainty level associated with the identified solution, given the measurement random error and the chosen filtering parameters.

Furthermore, it was shown in the proposed example that the errors were increasing near the edges and areas with large strain gradients; hence, the span R could be spatially adapted in order to better control the local identification errors.

Finally, the methodology should be applied to the identification of nonlinear constitutive laws in future works.

References

Amiot F, Hild F and Roger J P 2006 Identification of elastic property and loading fields from full-field measurements *Int. J. Solids Struct.* **44** 2863–87

Avril S, Feissel P, Pierron F and Villon P 2008a Estimation of the strain field from full-field displacement noisy data. Comparing finite elements global least squares and polynomial diffuse approximation *Eur. J. Comput. Mech.* **17** 857–68

Avril S *et al* 2008b Identification from measurements of mechanical fields *Exp. Mech.* **48** 381–402

Badulescu C 2010 Calcul précis des déformations planes par la méthode de la grille, application à l'étude d'un multicristal d'aluminium *PhD Thesis* Univeristé Blaise Pascal, Clermont-Ferrand

Ben Azzouna M, Feissel P and Villon P 2013 Modified constitutive relation error strategy for elastic properties identification *Experimental and Applied Mechanics* vol 4 (*Conf. Proc. Society for Experimental Mechanics Series* vol 34) (New York: Springer) pp 221–8

Ben Azzouna M, Périé J N, Guimard J M, Hild F and Roux S 2011 On the identification and validation of an anisotropic damage model using full-field measurements *Int. J. Damage Mech.* **20** 1130–50

Bonnet M and Constantinescu A 2005 Inverse problems in elasticity *Inverse Problems* **21** R1–R50

Bornert M *et al* 2009 Assessment of digital image correlation measurement errors: methodology and results *Exp. Mech.* **49** 353–70

Brancherie D, Villon P, Ibrahimbegovic A, Rassineux A and Breitkopf P 2006 Transfert de champs par approximation diffuse avec conservation de l'énergie *Eur. J. Comput. Mech.* **15** 107–18

Breitkopf P, Rassineux A and Villon P 2002 An introduction to moving least squares meshfree methods *Rev. Eur. Elém. Finis* **11** 825–67

Claire D, Hild F and Roux S 2002 Identification of damage fields using kinematic measurements *C. R. Méc.* **330** 729–34

Collins J C, Hart G C and Kennedy B 1974 Statistical identification of structures *AIAA J.* **12** 185–90

Cottin N, Felgenhauer H P and Natke H G 1984 On the parameter identification of elastomechanical systems using input and output residuals *Arch. Appl. Mech.* **54** 378–87

Deraemaeker A, Ladevèze P and Romeuf T 2004 Model validation in the presence of uncertain experimental data *Eng. Comput.* **21** 808–33

Dhatt G, Lefrançois E and Touzot G 2012 *Finite Element Method* (New York: Wiley)

Feissel P 2012 From displacement to strain *Full-Field Measurements and Identification in Solid Mechanics* ed M Grédiac and F Hild (New York: Wiley) pp 191–222

Feissel P and Allix O 2007 Modified constitutive relation error identification strategy for transient dynamics with corrupted data: the elastic case *Comput. Methods Appl. Mech. Eng.* **196** 1968–83

Feissel P, Henry J, Ben Azzouna M and Aboura Z 2011 Space-time diffuse approximation filtering: application to early and fatigue damage detection in interlock composites *Photomechanics (Brussels, Belgium, 7–9 Feb.)*

Francis D, James S W and Tatam R P 2007 Surface strain measurement using multi-component shearography with coherent fibre-optic imaging bundles *Meas. Sci. Technol.* **18** 3583–91

Geers M, Borst R D and Brekelmans W 1996 Computing strain fields from discrete displacements in 2D-solids *Int. J. Solids Struct.* **33** 4293–307

Gras R, Leclerc H, Roux S, Otin S, Schneider J and Périé J N 2012 Identification of the out-of-plane shear modulus of a 3D woven composite *Exp. Mech.* doi:10.1007/s11340-012-9683-4

Grédiac M, Pierron F, Avril S and Toussaint E 2006 The virtual fields method for extracting constitutive parameters from full-field measurements: a review *Strain* **42** 233–53

Hemez F and Farhat C 1993 Updating finite element dynamic models using element-by-element sensitivity methodology *AIAA J.* **31** 1702–11

Hild F and Roux S 2006 Digital image correlation: from displacement measurement to identification of elastic properties—a review *Strain* **42** 69–80

Kavanagh K T and Clough R W 1971 Finite element applications in the characterization of elastic solids *Int. J. Solids Struct.* **7** 11–23

Kobayashi A S 1987 *Handbook on Experimental Mechanics* (New York: Wiley)

Ladevèze P, Reynier M and Maya N 1994 Error on the constitutive relation in dynamics *Inverse Problems in Engineering* ed H D Bui and M Tanaka (Rotterdam: Balkema) pp 251–6

Leclerc H, Périé J N, Roux S and Hild F 2009 Integrated digital image correlation for the identification of mechanical properties *Lect. Notes Comput. Sci.* **5496** 161–71

Nayroles B 1994 Using the diffuse approximation for optimizing the location of anti-sound sources *J. Sound Vib.* **171** 1–21

Nayroles B, Touzot G and Villon P 1991a La méthode des éléments diffus *C. R. Acad. Sci., Paris* II **313** 133–8

Nayroles B, Touzot G and Villon P 1991b L'approximation diffuse *C. R. Acad. Sci., Paris* II **313** 293–6

Pagnacco E, Lemosse D, Hild F and Amiot F 2005 Inverse strategy from displacement field measurement and distributed forces using FEA *SEM Annu. Conf. and Exposition on Experimental and Applied Mechanics (Portland)*

Prax C, Sadat H and Salagnac P 1996 Diffuse approximation method for solving natural convection in porous media *Transport Porous Media* **22** 215–23

Réthoré J, Roux S and Hild F 2009 An extended and integrated digital image correlation technique applied to the analysis of fractured samples *Eur. J. Comput. Mech.* **18** 285–306

Roux S and Hild F 2008 Digital image mechanical identification *Exp. Mech.* **48** 495–508

Sadat H and Prax C 1996 Application of the diffuse approximation for solving fluid flow and heat transfer problems *Int. J. Heat Mass Transfer* **39** 214–8

Sutton M A, Orteu J J and Schreier H 2009 *Image Correlation for Shape, Motion and Deformation Measurements* (London: Springer)

Villon P, Borouchaki H and Saanouni K 2002 Transfert de champs plastiquement admissibles *C. R. Méc.* **330** 313–8

Zavattieri P, Savic V, Hector L G Jr, Fekete J R, Tong W and Xuan Y 2009 Spatio-temporal characteristics of the Portevin–Le Châtelier effect in austenitic steel with twinning induced plasticity *Int. J. Plast.* **25** 2298–330